IET Renewable Power Generation

WILEY

IET The Institution of Engineering and Technology

ORIGINAL RESEARCH OPEN ACCESS

Artificial-Intelligence-Based Reduced Sensor Voltage Control Strategy for DC Microgrid Applications

Hussain Sarwar Khan | Kimmo Kauhaniemi

School of Technology and Innovations, University of Vaasa, Vaasa, Finland

Correspondence: Hussain Sarwar Khan (hussain.khan@uwasa.fi)

Received: 10 December 2024 | **Revised:** 8 May 2025 | **Accepted:** 26 May 2025

Funding: This work is carried out in a project titled Smart Grid 2.0 with the financial support provided by Business Finland under Grant No. 1386/31/2022.

ABSTRACT

The expeditious advancement in renewable energy technologies enables the concept of microgrids to boost the incorporation of renewable energy into power systems. In this context, distributed generation (DG)-based DC microgrids (MGs) are favoured because of their higher efficiency, greater reliability, and simpler development and control compared to their AC counterparts. This paper presents an artificial neural network (ANN) voltage control for a DC-DC step-up converter to reduce the number of sensors in the DC microgrids. The proposed approach offered cost-effective and better voltage regulation in multi-bus DC MG. The proposed methodology employs quasi-stationary line (QSL) modeling to account for DC MG uncertainties and disturbances, while simultaneously developing and implementing a model predictive voltage control (MPVC) strategy to generate the comprehensive dataset. The converter's voltage error and switching signals, extracted from the generated dataset, serve as input features for offline training of an artificial neural network (ANN). Once trained, the ANN is deployed online to regulate distributed generators (DGs) within a multi-bus DC MG. Real-time hardware-in-the-loop simulations using OPAL-RT 4510 demonstrate that the proposed controller effectively regulates voltage with reduced sensors, ensuring improved reliability and efficiency.

1 | Introduction

With the development and advancement of renewable energy technology, modern power systems have become more complex and have undergone extensive changes over the past two decades. Microgrids (MGs) offer a promising solution for the effective integration of renewable energy resources. As crucial smart grid components, these systems will provide carbon-free and sustainable energy to consumers while operating in grid-tied and islanded modes. However, electrical systems are predominantly based on alternating current (AC). Advancements in power electronics technology have made direct current (DC) systems more efficient at all levels, namely generation, distribution, and transmission, and capable of operating in a wide range of voltages.[1]. The advantages of DC MG over AC MG can be summarized as:

- Most renewable energy resources, such as fuel cells, photovoltaic (PV) systems, and battery energy storage systems (BESS), generate DC power. Although wind turbines produce AC power, they can be effectively integrated into DC MGs because of the availability of advanced power converters.
- Most energy storage systems (ESS) are inherently DC-based. This characteristic facilitates easier integration of ESS into DC MGs, resulting in reduced costs, higher efficiency, simpler control, and improved reliability.
- The overall control of DC MGs is simpler due to the absence of factors such as frequency regulation, reactive power management, voltage imbalance, and harmonics.

Due to the advantages above, the DC MG is a well-accepted solution for the utility grid and the transportation sector, such as

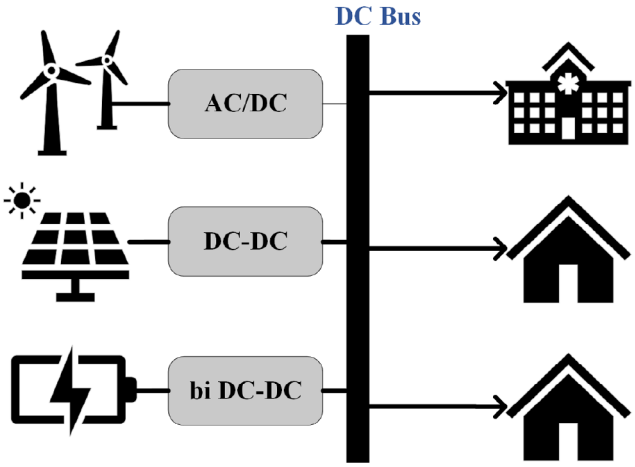

FIGURE 1 | The typical configuration of an autonomous DC microgrid has DG units, ESS, loads, and their control.

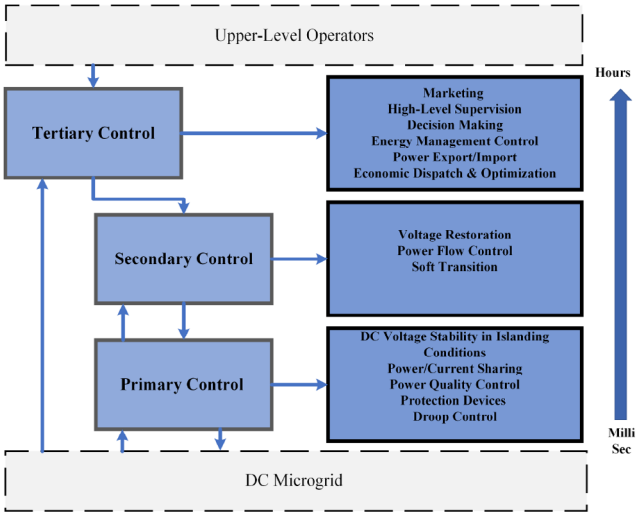

FIGURE 2 | Control architecture description for autonomous DC microgrid.

electric ships and aircraft. Figure 1 illustrates the typical DC MG configuration that contains multiple sources such as photovoltaic panels (PV), wind turbine (WT), and energy storage systems (ESS), which are connected to a common DC bus through a power electronic interface (PEI). The distribution network topology of DC microgrids (MGs) can vary, from radial to ring-type distribution systems.

The primary responsibilities of the control system in a DC microgrid (DC MG) are to address the following issues [2]:

- Regulation of DC-bus voltage.
- Accurate power sharing among the distributed generators (DGs)
- Management of power quality issues.
- Coordination among the distributed energy resources and energy storage systems (ESS).
- Unit commitment and economic dispatch of the DC MG.
- Minimization of transmission losses.
- Utilization of DERs to their full potential.

To address the aforementioned issues, the hierarchical control strategy has garnered significant attention due to its multi-layered architecture. This strategy comprises three layers: primary, secondary, and tertiary control, as illustrated in Figure 2. The primary layer includes an inner control loop to regulate the voltage and current of the converter, while droop control is employed to share power among the distributed energy resources (DER). The secondary control layer is responsible for voltage compensation and improving power-sharing accuracy. At the highest level, the tertiary control layer handles economic dispatch, system optimization, and energy management within the DC microgrid. However, this paper focuses exclusively on primary control; the secondary and tertiary controls are not studied here.

Numerous strategies for coordinating multiple distributed generators (DGs) in the autonomous mode of microgrids (MGs) have been proposed in existing research [3]. These strategies include master-slave control [4], load-sharing techniques [5, 6], centralized control [7], and others. These methods typically rely on a communication network among the DGs to ensure efficient and stable operation; however, this requirement adds complexity and can potentially reduce the system's reliability. Consequently, implementing a method like droop control is essential for accurate power sharing among DGs. In [8], the authors introduce decentralized droop control as a beneficial strategy, eliminating the need for an external communication link between power electronic interface-based DGs. The primary objectives of droop control in DC MGs are to share power between DGs and maintain voltage stability at the DC bus. In this context, the droop control functions as the external loop of the power converter, while the voltage control strategies are applied within the inner loop of the DG in the MG.

In the realm of power electronics (PE) control, the research community has extensively explored various linear controllers, notably PI and PID, which are widely implemented as evidenced by numerous studies and are widely used by the PE industry [9, 10]. Despite their prevalent use, these linear theory-based controllers exhibit enormous practical limitations, such as PID parameter tuning, limited ability to reject disturbances, operating point shifts towards instability due to parameter variations, and an inability to address the nonlinear characteristics of power systems adequately.

To address the shortcomings of linear controllers and improve the transient behaviour, various nonlinear control strategies like sliding mode control (SMC), fuzzy-logic control (FLC), and model predictive control (MPC) have been developed. For instance, a fuzzy-logic control approach for DC converters in photovoltaic lighting systems is studied in [11]. The microcontroller implemented the fuzzy logic for the DC power converter, which was explored in [12]. FLC primarily operates on if-else logic, and its response depends on pre-established rules without requiring a mathematical model of the system, adeptly managing nonlinearities. The performance of fuzzy controllers for the DC-DC

converter is also effective across a range of operating conditions. However, the reliability of fuzzy controllers is often questioned due to the lack of formal analysis. Therefore, numerous control approaches are amalgamated in the literature to address the limitations of fuzzy logic control [13].

Sliding mode control and model predictive control have been extensively proposed in the literature and have shown promising results in power electronic converter applications. Based on the principles of variable structure control theory, sliding mode control involves two main phases: the reaching phase, where system state trajectories are directed to a predefined sliding surface, and the sliding phase, where they remain within this surface based on predefined criteria. Despite its resilient performance, robustness to parametric variations, and excellent transient response under various loads, its implementation faces significant challenges. It includes issues such as chattering phenomena, high switching losses, and the complexity of its mathematical modelling as the sliding order increases [14, 15]. In [3], the authors presented the intelligent sliding mode control for parallel converters in DC microgrid for constant power load applications.

Model predictive control (MPC) is a digital control strategy that fundamentally differs from traditional linear control methods. Unlike linear controllers, which typically require separate loops for each controlled variable and their subsequent cascading, MPC leverages a discrete-time model of the converter and its filter to predict outcomes for all potential input combinations. The input that minimizes a predefined cost function is selected for the next sampling period. It is typically defined as the square of the Euclidean distance between the measured and reference signals [16]. MPC-based control schemes have been proposed for a wide range of applications, including AC systems [17, 18], DC systems [19, 20], and hybrid microgrids (MGs) [21, 22]. In AC/DC and AC MGs, MPC strategies have been developed for bidirectional DC/DC converters [18] and AC/DC converters [21, 23]. In the context of DC microgrids, MPC has been employed to enhance stability, optimize power sharing, manage energy systems, improve transient response, and address pulsed power loads in naval DC MGs. Additionally, MPC is used to control DC/DC converters, maximize photovoltaic (PV) power output through maximum power point tracking, and reduce power losses in DC MGs. However, MPC's effectiveness heavily depends on the system's mathematical model's accuracy and has significant computational burden. Moreover, it has a variable switching frequency, which can be a limitation in some applications. To address this, recent research has introduced MPC methodologies that maintain a constant switching frequency, tailored for various power electronic applications [16].

Data-driven or model-free control methods, particularly those utilizing artificial neural networks (ANN), are becoming increasingly common in the field of power converter control [24]. ANN-based control techniques are proposed for voltage sag classification, fault detection, short-term prediction, etc. ANN-based converter control has been proposed in [25, 26]. In [27], neural network predictive-based voltage control has been introduced for the DC-DC buck converter. PID controller data serve as training data to train ANN. Once trained, neural network predictive control (NNPC) regulates the voltage. An NNPC controller designed for a grid-connected synchronverter is presented in [28]. Furthermore, an improved control strategy has been proposed that combines a proportional-integral controller with an ANN to improve performance metrics such as overshoot, rise time, and settling time [29]. A fuzzy logic-aided ANN power oscillation damping controller is proposed for hybrid AC/DC MG [30]. Sliding mode robust droop control scheme enhanced by an ANN algorithm for islanded photovoltaic-integrated microgrids is studied in [31]. In [32], the author studied the ANN-based control for nonlinear DC microgrids. Real-time FPGA-based validation of ANN for DC-DC converter is illustrated in [33].The superiority of the ANN controller over other controllers is due to the various key advantages [34]:

- It eliminates the need for a mathematical model of the system.
- Its performance can be enhanced through controller tuning.
- Its design does not necessitate specialized expertise.

This study introduces an innovative reduced-sensor ANN-based voltage control technique for distributed generations in a DC microgrid, specifically focusing on a DC-DC step-up (boost) converter. Our methodology employs an artificial neural network (ANN) that requires fewer sensors compared to model predictive control, which typically requires at least two sensors. Table 1 summarizes the overall features of various existing reduced sensor control techniques. A quasi-stationary line (QSL) approximation is used to model the uncertainties, disturbances, and line dynamics of the DC MG, as studied in [40]. Initially, model predictive control (MPC) is implemented for the DC-DC converter as a parent control method and also as a tool to extract a dataset comprising input features such as voltage, current, power, and switching pulses under different loading and operating conditions. After extracting the dataset, various combinations of input features are evaluated to identify the most effective for control purposes. The error between the output and reference voltage is ultimately selected as the primary input feature. At the same time, the converter's switching action is chosen as the output feature for the artificial neural network (ANN) in this study. The selected input-output pair simplifies the system to a single input and single output (SISO) configuration, reducing the computational complexity [41] and enabling efficient training of the ANN. The SISO ANN is trained offline using the Bayesian regularization technique, with performance validated through metrics such as mean squared error (MSE) and confusion matrices. Upon achieving high accuracy and reliability during the training, validation, and testing phases, the ANN is integrated into the Simulink environment for control of the Boost converter. Figure 7 illustrates the overview of the proposed control strategy: the training phase combines using MPC to anticipate the converter output voltage and collection of state variables data under full-state observation. The data collected are used to train the ANN. In the test phase, the trained neural network is employed online to control the converter's output voltage instead of the MPC. The simulation results validate the superiority of the proposed ANN-based control strategy, demonstrating enhanced voltage regulation performance and accuracy compared to conventional PI controllers and the model predictive control (MPC) method used in this study. Furthermore, real-time HIL simulations were conducted using the OPAL-RT 4510 platform to assess the controller's effectiveness under various test scenarios, including plug-and-play events, microgrid

TABLE 1 | Overview of sensorless control approaches for DC MG.

References	[29, 35]	[36]	[37]	[38]	[39]	Proposed
Controller	Deep learning	Lyapunov based state observer	Pre-defined objective function	Fifth dimensional estimator	Proportional derivative (PD)	ANN
Load variation	✓	✓	✓	✓	✓	✓
PnP	—	✓	—	—	—	✓
Parametric variations	—	—	—	✓	—	✓
Stability analysis	—	✓	✓	✓	—	✓
Application	PV converter	DC MG	Buck-boost converter	AC-DC converter	DC/DC boost converter	DC/DC boost converter
Sensor reduction	Current	Current, voltage	Current	Current	Current	Current

topology reconfiguration, and responses to unknown load variations. The proposed controller exhibits robust performance in both simulation and hardware-in-the-loop (HIL) environments. Reducing the number of sensors improves system reliability by minimizing potential failure points and improves speed by eliminating communication delays associated with sensors. This leads to a more responsive and efficient system. Additionally, current sensors are generally more susceptible to failure in DC systems than voltage sensors because of their higher exposure to thermal and electrical stresses. Therefore, favoring voltage sensors over current sensors increases the system's resilience and ensures more reliable operation in case of sensor failure. The following are the key features of the proposed approach:

1. Whole system dynamics are incorporated by using QSI approximation.
2. The ANN is implemented by designing the control objectives based on MPC.
3. ANN architecture is developed by merging the feedback from the DC/DC converter with the ANN, creating a unified system.
4. The training of ANN is carried out offline to prevent any stability issues.

The rest of the paper is organized as follows: Mathematical modeling of the DC MG is developed in Section 2, and the basic principle of model predictive control is explained in Section 3. Section 4 delves into the artificial neural network and the training process of the ANN model. Simulation and HIL results are discussed in Section 5. Finally, the paper summarizes the key findings and insights in Section 6.

2 | Mathematical Model of Islanded DC Microgrid

Figure 1 illustrates the configuration of the DC microgrid. Usually, a DC microgrid can consist of PV arrays, wind turbines, fuel cells connected with the bus through a unidirectional DC/DC converter, an energy storage system with a bidirectional DC/DC converter, and fixed and variable DC loads. It may also have an AC load connected via a DC/AC converter. There is the possibility of connecting the DC MG with the AC utility grid through a bidirectional interlink AC/DC converter. The DC MG controls are divided into three types based on communication: decentralized control, centralized control, and distributed control.

The equivalent circuit diagram of the DC-DC boost converter is shown in Figure 3, where V_{in_i} represents the input voltage, which models renewable energy such as PV systems, batteries,

FIGURE 3 | Equivalent circuit diagram of step-up converter.

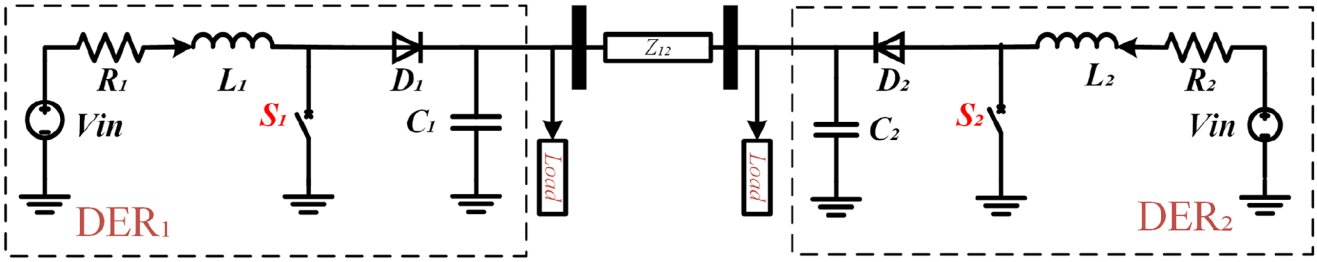

FIGURE 4 | Schematic diagram of an autonomous DC microgrid with two DERs.

etc. Due to the uncertainty in the system load ratings, the system is modelled as a current disturbance i_l. The output of DER_j is denoted as V_{out_j}, while DER_i is represented as V_{out_i}. Other parameters follow a similar notation pattern. Additionally, $d(t)$ represents the duty cycle at the switching instant t in the DC-DC converter. The dynamic response of DER_i and $Line_{ij}$ is determined using Krichoff's current and voltage laws, and their equation are expressed as follows:

$$\frac{dV_{cli}}{dt} = \frac{1}{C_{fi}} i_{L_{1i}} - \frac{1}{C_{fi}} i_{L_{1i}} d(t) - \frac{1}{C_i} i_{pci} + \frac{1}{C_i} i_{ij} \tag{1}$$

$$\frac{di_{Li}}{dt} = -\frac{R_{1i}}{L_{1i}} i_{Li} - \frac{V_{cli}}{L_{1i}} + \frac{V_{cli}(t)}{L_{1i}} d(t) + \frac{V_{in_i}}{L_{1i}} \tag{2}$$

$$Line_{ij} = \frac{dI_{ij}}{dt} = \frac{V_{in_j}}{L_{ij}} - \frac{V_{in_i}}{L_{ij}} - \frac{R_{ij} I_{ij}}{L_{ij}} \tag{3}$$

The DER unit parameters C_{fi}, R_{1i} and L_{1i} are the LC parameters of the circuit. Moreover, the line parameters are specified as $L_{ij} = L_{ji}$ and $R_{ij} = R_{ji}$, ensuring symmetry between the connecting lines and currents flowing between the nodes are equal in magnitude but opposite in directions, maintaining the consistency with the Kirchoff's current law.

2.1 | Quasi-Stationary-Line (QSL) Model Approximation

The Quasi-Stationary Line (QSL) model is an approximation used to simplify the analysis of the system by assuming that changes in the system occur over a period long enough for the system to be considered quasi-static yet short enough to prevent it from reaching full equilibrium. In the short transmission line, the line's inductance is relatively small and has a small time constant, allowing the line dynamics to be neglected. Consequently, the rate of change of the inductors' current over time $\frac{dI_{ij}}{dt}$ is negligible and also expressed as QSL approximations [42]. So, This QSL model approximation is only valid for short transmission lines. A comprehensive model based on the quasi-stationary line (QSL) approximation should be developed for medium and long transmission lines to accurately capture electrical behavior and dynamic characteristics over extended distances. Figure 4 illustrates the two coupled distributed energy resource (DER) units, consisting of a DC-DC converter, input source V_{in}, and the local load connected through a line, denoted as "ij," with resistance R_{ij} and inductance rmL_{ij}, respectively. The proposed control scheme applies to DC microgrids (MG) with radial, parallel, and meshed topologies in this configuration. In this study, a DC-DC boost converter with uncertainties is considered. Based on this assumption, Equation (4) is derived from Equation (3).

$$I_{ij} = \frac{V_{in_j} - V_{in_i}}{R_{ij}} \tag{4}$$

Substituting Equation (4) to Equation (1) gives the QSL approximation of DER_i, expressed in Equation (5).

$$\mathrm{DER}_i := \begin{cases} \frac{\mathrm{dV_{c1_i}}}{\mathrm{dt}} = \frac{(1-d_i)}{C_{f_i}} I_{L_i} + \frac{V_{\mathrm{c1}_j}}{R_{\mathrm{ij}} C_{f_i}} - \frac{V_{\mathrm{c1}_i}}{R_{\mathrm{ij}} C_{f_i}} - \frac{1}{C_{f_i}} i_{L_i} \\ \frac{\mathrm{di}_{L_i}}{\mathrm{dt}} = \frac{1}{L_{1_i}} V_{\mathrm{ini}} - \frac{(1-d_i)}{L_{1_i}} V_{\mathrm{c1_i}} - \frac{R_{1_i}}{L_{1_i}} i_{L_i} \end{cases} \tag{5}$$

$$DER_{[i]} = \begin{cases} \dot{\tilde{x}}_{[i]}(t) = A_{[ii}(t)\tilde{x}_{[i]}(t) + B_i(t)\tilde{u}_{[i]}(t) \\ \qquad + D_i(t)\tilde{w}_{[i}(t) + \tilde{\zeta}_{[i]}(t) \\ \tilde{y}_i(t) = C_i(t)\tilde{x}_{[i]}(t) \end{cases} \tag{6}$$

The generalized state space representation of QSL is given in Equation (6). This formulation represents a small-signal state vector, which includes the perturbed system variables. The input $\tilde{u}(t) = \tilde{d}_i(t)$, corresponds to the duty cycle of DER_i. The term $\tilde{w}_{[i]}(t) = \left[\tilde{L}_{L_i}, \tilde{v}_{\mathrm{in}_i}\right]^{\top}$ are small-signal exogenous disturbances, accounting for variations in current and input voltage. Additionally, $\tilde{\zeta}_{[i]}(t) = A_{ij}(t)\tilde{x}_j$ captures the coupling between DER_i and DER_j, indicating the interaction between different distributed energy resources. $\tilde{y}_{[i]}(t)$ is the output vector, which is the function of the system state variables. Equation (5) is rewritten as a state space model and described below.

$$A_{ii}(t) = \begin{bmatrix} \frac{-1}{R_{ij} C_{f_i}} & \frac{(1-\bar{D}_i)}{C_{f_i}} \\ \frac{-(1-\bar{D}_i)}{L_{1_i}} & \frac{-R_{1_i}}{L_{1_i}} \end{bmatrix}, B_i(t) = \begin{bmatrix} \frac{-i_{L_i}}{C_{f_i}} \\ \frac{\bar{V}_{\mathrm{c1_i}}}{L_{1_i}} \end{bmatrix}$$

$$D_i(t) = \begin{bmatrix} \frac{-1}{C_{f_i}} & 0 \\ 0 & \frac{1}{L_{1_i}} \end{bmatrix}, A_{ij}(t) = \mathrm{diag}\left(\frac{1}{R_{ij} C_{f_i}}, 0\right), C_i = I_{2\times 2}$$

The linearised model's applicability in Equation (6) hinges on the premise that fluctuations around the equilibrium point are minor enough to ensure the inherent non-linear system. Equation (5) ensures the asymptotic stability of the system. However, if fluctuations and disturbances extend too high, the linearized representation of the system might lose its accuracy. Building on Equation (6), the small-signal state-space model

for the interconnected distributed energy resources depicted in Figure 4, is articulated as follows:

$$\begin{bmatrix}\dot{\hat{x}}_{[i]}\\ \dot{\hat{x}}_{[j]}\end{bmatrix} = \begin{bmatrix}A_{ii}(t) & A_{ij}(t)\\ A_{ji}(t) & A_{jj}(t)\end{bmatrix}\begin{bmatrix}\tilde{x}_{[i]}\\ \hat{x}_{[j]}\end{bmatrix} + \begin{bmatrix}B_i(t) & 0\\ 0 & B_j(t)\end{bmatrix}\begin{bmatrix}\tilde{u}_{[i]}\\ \tilde{u}_{[j]}\end{bmatrix} + \begin{bmatrix}D_i(t) & 0\\ 0 & D_j(t)\end{bmatrix}\begin{bmatrix}\tilde{w}_{[i]}\\ \tilde{w}_{[j]}\end{bmatrix} \quad (7)$$

$$\begin{bmatrix}\hat{y}_{[i]}\\ \hat{y}_{[j]}\end{bmatrix} = \begin{bmatrix}C_i & 0\\ 0 & C_j\end{bmatrix}\begin{bmatrix}\hat{x}_{[i]}\\ \hat{x}_{[j]}\end{bmatrix}$$

The model expressed in Equation (7) describes the interaction between various DER units through coupling terms and also considers the system disturbances. The output matrix $C_i = I_{2x2}$ ensures that the system outputs are directly proportional to the state variables.

Now expand the model for interconnected DER units, Let represent the set of all interconnected DER units and , $\mathcal{N}_i \subset \mathcal{D}$ is a neighbouring subset of DER_i, which is coupled via electrical links ij. The coupling between different DER units is expressed by the term $DER_{ij}\ \tilde{\xi}_{[i]}(t) = \sum_{j\in N_i} A_{ij}(t)\tilde{x}_{[j]}(t)$. Therefore, the matrix A_{ii} is reevaluated as:

$$A_{\mathrm{ii}}(t) = \begin{bmatrix}\sum_{j\in N_i}\dfrac{-1}{R_{ij}C_{f_i}} & \dfrac{(1-\bar{D}_i)}{C_{f_i}}\\ \dfrac{-(1-\bar{D}_i)}{L_{1_i}} & \dfrac{-R_{1_i}}{L_{1_i}}\end{bmatrix}$$

The small-signal linear time-variant model of the whole system, including the disturbances, coupling, and dynamics in the compact form, is represented as:

$$\begin{cases}\dot{\tilde{\mathbf{x}}}(t) = \mathbf{A}(t)\tilde{\mathbf{x}}(t) + \mathbf{B}(t)\tilde{\mathbf{u}}(t) + \mathbf{D}(t)\tilde{\mathbf{w}}(t)\\ \tilde{\mathbf{y}}(t) = \mathbf{C}(t)\tilde{\mathbf{x}}(t)\end{cases}$$

Where $\tilde{\mathbf{x}}, \tilde{\mathbf{u}}, \tilde{\mathbf{w}}, \tilde{\mathbf{y}}$ are defined as:

$$\tilde{\mathbf{x}} = \begin{bmatrix}\tilde{x}_{[1]}\\ \tilde{x}_{[2]}\\ \vdots\\ \tilde{x}_{[N]}\end{bmatrix},\quad \tilde{\mathbf{u}} = \begin{bmatrix}\tilde{u}_{[1]}\\ \tilde{u}_{[2]}\\ \vdots\\ \tilde{u}_{[N]}\end{bmatrix},$$

$$\tilde{\mathbf{w}} = \begin{bmatrix}\tilde{w}_{[1]}\\ \tilde{w}_{[2]}\\ \vdots\\ \tilde{w}_{[N]}\end{bmatrix},\quad \tilde{\mathbf{y}} = \begin{bmatrix}\tilde{y}_{[1]}\\ \tilde{y}_{[2]}\\ \vdots\\ \tilde{y}_{[N]}\end{bmatrix},$$

$$\mathbf{B}(t) = \mathrm{diag}\,(B_i(t)),$$

$$\mathbf{D}(t) = \mathrm{diag}\,(D_i(t)),$$

$$\mathbf{C} = \mathrm{diag}\,(C_i),$$

$$\mathbf{A}(t) = \begin{bmatrix}A_{11}(t) & A_{12}(t) & \dots & A_{1N}(t)\\ A_{21}(t) & A_{22}(t) & \dots & A_{2N}(t)\\ \vdots & \vdots & \ddots & \vdots\\ A_{N1}(t) & A_{N2}(t) & \dots & A_{NN}(t)\end{bmatrix}$$

The matrices $\mathbf{B}(t)$, $\mathbf{D}(t)$, $\mathbf{C}(t)$, and $\mathbf{A}(t)$ are block diagonal, representing the local dynamics of each DER unit. The system matrix $\mathbf{A}(t)$ includes the DER's internal dynamics and the coupling between different DER units.

3 | Model Predictive Control for DC-DC Converter

Developing a discrete-time model for the DC converter is essential to implement MPC. The circuit diagram of the step-up boost converter is presented in Figure 4. The output voltage of this step-up DC converter is regulated by adjusting the duty cycle of the pulse width modulation (PWM) signal. A significant limitation of MPC is its variable switching frequency, which can present challenges in specific applications. Where S_1 is a controllable switch, R_1 is the damping resistance, and current through inductor L is i_{L1} and the voltage across the capacitor C_1 is v_{C1}. V_{in} represents the input voltage of the DC source. A second-order low-pass filter is utilized to reduce high-frequency components in the signal. Equation (8) describes the inductive behaviour, while Equation (9) explains the capacitive nature of the system:

$$\frac{di_{Ll}(t)}{d(t)} = -\frac{R_1}{L_1}i_{Ll}(t) - \frac{V_{cl}(t)}{L_1} + \frac{V_{cI}(t)}{L_1}u(t) + \frac{V_{\mathrm{in}}}{L_1} \quad (8)$$

$$\frac{dV_{cl}(t)}{d(t)} = \frac{1}{C_1}i_{L_1}(t) - \frac{1}{C_1}i_{L_1}(t)u(t) - \frac{1}{R_1C_1}V_{cl}(t) \quad (9)$$

The function $u(t)$ defines the switch states as presented in Equation (10). When the switch S_1 is equal to 1 and is in the ON state, whereas if S_1= 0, it is deemed to be in the OFF state.

$$u(t) = \begin{cases}0 & S_1 = 0\\ 1 & S_1 = 1\end{cases} \quad (10)$$

The discrete-time model of the DC converter is presented in Equations (11) and (12). These equations are formulated to predict the future behavior of voltage and current, and they are derived from Equations (6) and (7) and Equations (11) and (12).

$$i_{l1}(k+1) = \left(\frac{TR_1}{L_1} - 1\right)i_{L1}(k) + (u(k)-1)\frac{T}{L_1}V_{cl}(k) \quad (11)$$

$$V_{c1}(k+1) = \frac{T}{C_1}i_{Ll}(k) + \left(1 - \frac{T}{C_1R}\right)V_{c1}(k) - \frac{T}{C_1}i_{L1}(k)u(k) \quad (12)$$

Where the next (coming) instant is demonstrated by the term (k+1), the T represents the sampling time.

The development of model predictive control critically involves formulation of the cost function, which is determined by the positive value of the error between the reference and the predicted state parameter value. In this study, the single objective CF is

chosen and expressed in Equation (13).

$$J(k+1) = \left(V_c^*(k)^2 - V_{c1}(k+1)\right)^2 \tag{13}$$

The execution of the MPC algorithm to acquire the dataset is as follows:

- At the beginning of the switching instant, the converter's current and voltage are measured using sensors.
- Equations (11) and (12) are utilized to predict the state parameter at the next instant for all possible switching states, and then the CF is calculated using Equation (13) for each possible state.
- The state in which the CF attains its minimum value is selected to determine the switch position of the converter in the upcoming instant.

The data set acquired from the MPVC for the DC/DC converter is used to train the ANN.

4 | Implementation of Artificial Neural Network

Implementing linear control, such as PI, is easy and cost-effective. However, it cannot capture all the power system dynamics, especially when integrating renewable energy and complex loads such as CPL and impedance loads. These additions bring more uncertainties and non-linearities in modern power systems. Consequently, there is a need for more intelligent control schemes that provide robust performance across a wide range of operating conditions and are capable of managing and addressing the issues mentioned above. In this context, artificial intelligence and machine learning offer promising solutions. These advanced techniques can adapt to complex system behaviours and understand dynamics from data patterns. By leveraging AI, modern control approaches can achieve resilience, efficiency and greater flexibility as required by the modern power system. An artificial neural network (ANN) is a computational model inspired by the structure and function of human neural networks. It is a key technique within the broader field of machine learning and is designed to model complex relationships between inputs and outputs (targets). ANN models use learning algorithms to identify patterns in historical data, enabling them to make intelligent decisions and predictions. Figure 5 depicts the basic structure of multi-input and single output ANN. where M represents the input features ($\forall_m = \{1, \ldots., M\}$) and y is single output. It consists of several interconnected layers of artificial neurons, also referred to as nodes. The typical structure of ANN is divided into three layers, that is, input layer, hidden layer, and output layer. The input layer corresponds to features or raw data sets. In the input layer, the neuron represents each feature. Each input x_m is multiplied by the weighting factor $w_m(\forall_j = \{1, \ldots., j\})$ and added to the hidden layer. Hidden layers are responsible for processing and transforming information from the input layer by defining weights and activation functions to learn the complex patterns between inputs and outputs. The number of hidden layers depends upon the complexity of the problems. The output layer gives output or predictions based on previous knowledge. The ANN-based PV monitoring system is proposed in [43]. An ANN-based algorithm has been developed to detect cyber attacks in [44]. In [25], authors proposed MPC-aided ANN-based voltage control for 2-level VSC to attain better performance and lower THD. Furthermore, ANN-based MPC for a three-level flying capacitor converter is studied in [41] to prove the reduction of MPC computation burden using ANN. The ANN is considered a power tool for forecast and estimation in different power applications. This study aims to illustrate the implementation of ANN-based voltage control for DER unit in a DC microgrid with a reduced number of sensors and its effectiveness over a wide range of operations. In order to implement the ANN, The MPC-based voltage control is implemented for a step-up DC-DC converter to collect the error data between measured and reference voltage and output switching states having other characteristics such as load shift, change in input voltages, etc. By choosing these parameters, the single input and single output feed-forward ANN is developed

In this study, the single input and single output feed-forward ANN is implemented to reduce the computational burden and complexity and achieve better results while preserving all characteristics of the parent technique.

The output of a single neuron is mathematically expressed as:

$$y = \mathrm{Act}\left(b + \sum_{i=1}^{M} x_i w_i\right), \tag{14}$$

where $Act(.)$, w_i, b, and M are the activation function, weights of each input x_i, bias or correction factor, and the number of input elements (or neurons) where the input features $x = \{x_1, x_2, \ldots, x_M\}$, respectively. The most commonly used types of activation functions are hyperbolic tangent, softmax, linear, and sigmoid) [45]. An FF-ANN layer is developed by joining the multiple neurons into a single layer. The general equation used to compute the output of the multi-input single-output FF-ANN can be expressed as:

$$\begin{aligned} y_1 &= Act\left(\sum_{j=1}^{J} {}^2w_{j1} h_j + {}^2b_1\right), \\ h_j &= Act\left(\sum_{m=1}^{M} {}^1w_{mj} x_m + {}^1b_j\right), \quad \forall j = \{1, \ldots, J\}, \end{aligned} \tag{15}$$

where y_1 is the output of the ANN, represents the weights of the hidden and output layers, J is the number of hidden layers, M represents the number of input neurons, and refers to the biases of the hidden and output layers, respectively.

4.1 | Training of ANN

This subsection outlines the steps involved in training the ANN. The training of ANN is divided into two phases: Offline and online. In the offline phase, MPVC is formulated, developed, and tested using Matlab/Simulink simulations. The data extraction process begins by collecting the inputs and outputs of the implemented control technique. Various tests, such as step changes in load, voltage references, and supply voltages, are conducted to characterize the parent control approach comprehensively. After gathering the raw data, the selection of inputs and targets for

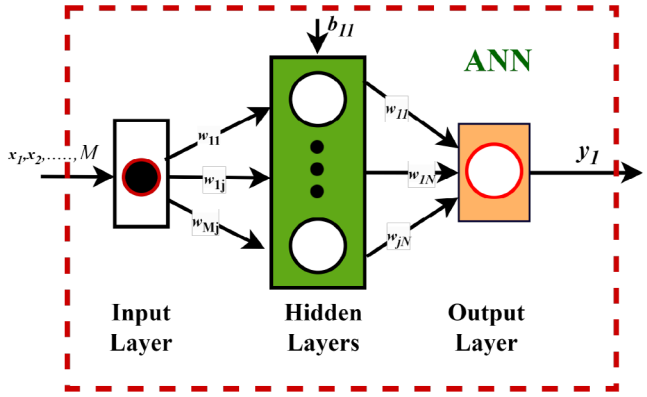

FIGURE 5 | Overview of multi-layer ANN with multi inputs and single output.

FIGURE 6 | Confusion matrix of the trained ANN based on the overall training data, where the correct and incorrect observations are highlighted in green and red, respectively.

training the ANN is based on a hit-and-trial method. The error between the output and reference voltage is ultimately chosen as the primary input feature, while the converter's switching action serves as the output feature in this study.The dataset selected for the offline training of the ANN consists of randomly sampled data from different reference voltage levels, including 90 V, 95 V, 100 V, and 105 V. The dataset is then randomly split into three subsets: training (70%), validation (15%), and testing (15%). The network is designed with ten hidden neurons, and training is performed using the Bayesian regularization technique, utilizing the "trainbr" function in MATLAB.

The confusion matrix visualizes and summarizes the performance of the trained ANN, as shown in Figure 6, which assesses the performance based on the network's output. In our case, the ANN outputs either 0 or 1, representing the pulse for the switch S1.The dataset comprises 180,006 samples in total. The acquired dataset consists of 78.78% samples from output class 1 and 21.22% from output class 0. The proposed controller successfully predicts the output class for random samples with an overall accuracy of 97.2% and a precision of 100% as expressed in Table 2. Table 3 compares the various control techniques, showcasing the number of sensors required for implementation. The MPC and multi-input ANN require two sensors to implement the methods. The proposed ANN technique only needs output voltage measurement, which makes it easy to implement and reduces hardware complexity.

TABLE 2 | Performance metrics of the model.

Metric	Value
Accuracy	97.2%
Precision (class 1)	100%
Recall (class 1)	96.5%
Specificity (class 0)	100%
F1 score (class 1)	98.2%

TABLE 3 | Comparison of sensor requirements for different control approaches.

Control technique	Features used	Inputs	Outputs
MPC	V_{in}, V_{out}, I_{out}	3	1
Multi-input ANN [26]	V_{in}, V_{out}, I_{out}	3	1
SISO ANN (proposed)	V_{out}	1	1

The trained ANN replaces MPC for real-time voltage control in the test phase. The trained ANN model is exported to Simulink to test its performance under the original scenario. To sum up, the complete procedure of the learning-based control strategy is illustrated in Figure 7, highlighting the key steps of the training and test phases. Additionally, Figure 8 visually represents the entire process. It is essential to mention that MPC accuracy relies on the system's mathematical modeling. However, the proposed control scheme does not require the system's model but a training dataset. It directly maps the raw input features to the desired outputs. Therefore, the performance of the ANN does not depend upon the system model or its parameters.

4.2 | Stability Analysis

Data-driven controls such as MPC-aided ANN have gained significant attention in control applications due to their ability to approximate complex nonlinear functions and comprehensively understand the system dynamics. The stability of control systems is a fundamental requirement to ensure predictable and reliable performance, unlike traditional control systems, where stability can be ensured through Lyapunov-based methods and recursive feasibility. ANNs present significant challenges due to their inherent nonlinearity, high-dimensionality, and data-driven nature, making formal stability proofs more complex. In [46], the authors propose a data-driven MPC scheme that ensures stability using Lyapunov analysis and recursive feasibility, using Hankel matrix representations for linear time-invariant (LTI)

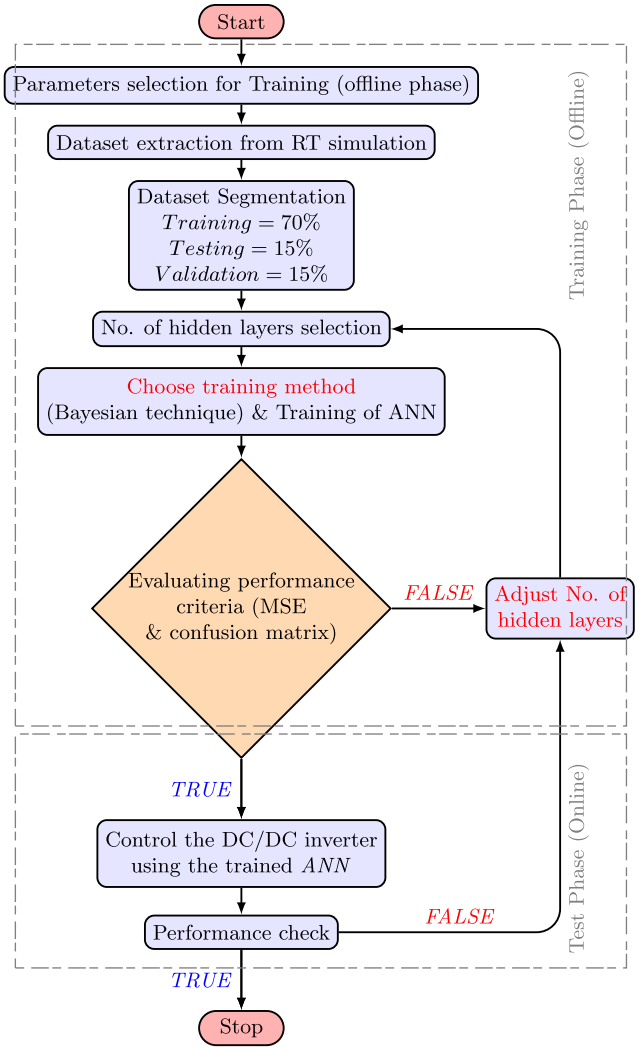

FIGURE 7 | Main steps in deploying the ANN-based control strategy for the DC/DC converter.

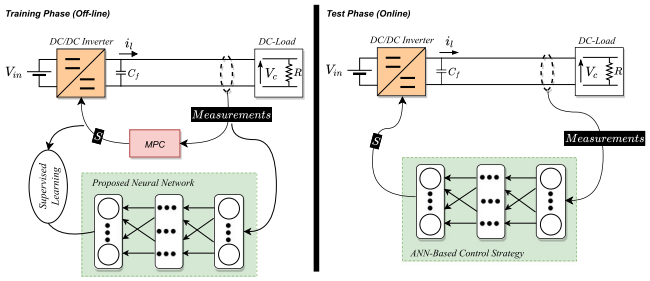

FIGURE 8 | Graphical overview of whole training process [26].

systems. However, applying similar stability guarantees to ANNs is challenging due to their non-convex optimization space, lack of explicit state-space models, and dynamic parameter updates via gradient descent. In [47], the authors analyze the robust stability of a data-driven MPC scheme without terminal constraints, proving practical exponential stability with a sufficiently long prediction horizon, even under noisy measurements. However, applying similar stability guarantees to ANNs is difficult due to their nonlinear activation functions, high-dimensional weight matrices, and stochastic updates, which complicate continuity

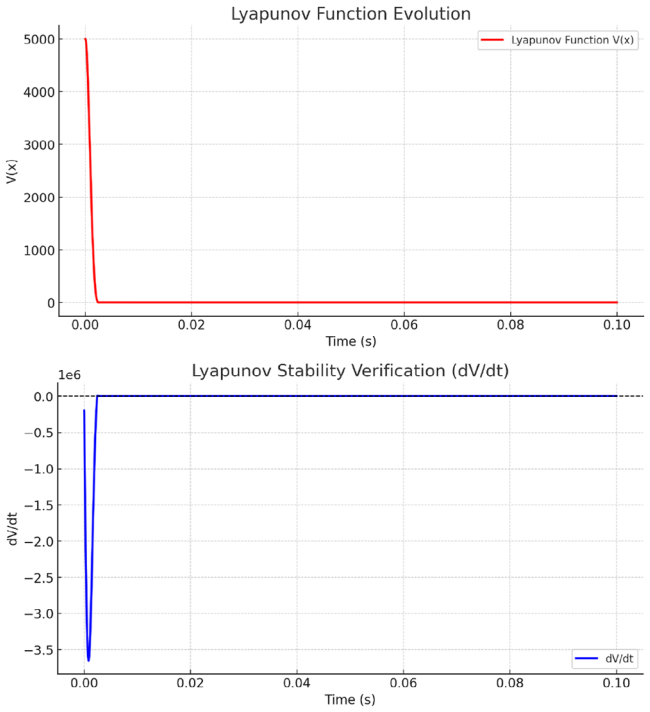

FIGURE 9 | Lyapunov stability verification plots. (a) Lyapunov function evolution. (b) Lyapunov stability verification.

and stability analysis. This study analyzes the controller's stability using Lyapunov's direct method. To validate the robustness of the ANN controller, we employ Lyapunov stability analysis and evaluate the system's convergence behavior through numerical simulations, as it is challenging to prove the mathematical stability of data-driven control techniques. A nonlinear system is considered Lyapunov stable if there exists a continuously differentiable Lyapunov function $V(x)$ satisfying:

- Positive definiteness: $V(x) > 0$ for all $x \neq 0$ and $V(0) = 0$, ensuring that the function measures system energy.
- Negative semi-definiteness: The time derivative $\dot{V}(x)$ satisfies $\dot{V}(x) \leq 0$, indicating that the energy of the system does not increase.
- Asymptotic stability: If $\dot{V}(x) < 0$, then $x \to 0$ as $t \to \infty$, ensuring that the system error vanishes over time.

The ANN controller's stability is evaluated by defining a quadratic Lyapunov function:

$$V(x) = \frac{1}{2} V_{\text{error}}^2 \tag{16}$$

where

$$V_{\text{error}} = V_{\text{ref}} - V_{\text{actual}} \tag{17}$$

Figure 9 shows the Lyapunov stability verification plots based on simulation data. Figure 9a presents the Lyapunov function $V(x)$ vs time plot. It can be observed from the figure that the Lyapunov function achieves the zero value in a short time, which means that the system stabilizes quickly. The controller effectively drives

the state toward equilibrium. consequently, the controller fulfills the key criteria and is considered asymptotic stable. Figure 9b demonstrates that the derivative of the Lyapunov function is also negative and decreases over time towards zero. We conclude that:

$$\frac{dV}{dt} \leq 0. \tag{18}$$

Since $\frac{dV}{dt} \leq 0$, the system satisfies the conditions for Lyapunov stability. Moreover, as $V_{\text{error}}(t) \to 0$ over time, the system is asymptotically stable.

4.3 | Discrete-Time Lyapunov Stability Analysis

The quadratic Lyapunov function in the discrete domain can be defined as:

$$L(k) = \frac{1}{2} V_{\text{err}}(k)^T V_{\text{err}}(k) \tag{19}$$

where $V_{\text{err}}(k) = V_{\text{ref}}(k) - V_{\text{actual}}(k)$. This function satisfies the following properties:

- Positive definite: $L(k) > 0$ for all $V_{\text{err}}(k) \neq 0$
- Zero at equilibrium: $L(k) = 0$ if and only if $V_{\text{err}}(k) = 0$

The change in the Lyapunov function between two discrete sampling instants is:

$$\Delta L(k) = L(k+1) - L(k) \tag{20}$$

$$\Delta L(k) = \frac{1}{2} V_{\text{err}}(k+1)^T V_{\text{err}}(k+1) - \frac{1}{2} V_{\text{err}}(k)^T V_{\text{err}}(k) \tag{21}$$

Assuming that V_{ref} remains constant due to small sampling time:

$$V_{\text{err}}(k+1) = V_{\text{ref}}(k) - V_{\text{actual}}(k+1) \tag{22}$$

The controller affects V_{actual} through the ANN model:

$$V_{\text{actual}}(k+1) = f(V_{\text{actual}}(k), \text{ANN}(V_{\text{err}}(k), i_L(k), V_{\text{in}}(k))) \tag{23}$$

The change in output voltage due to the controller can be approximated as:

$$V_{\text{actual}}(k+1) - V_{\text{actual}}(k) = \alpha \cdot V_{\text{err}}(k) \tag{24}$$

where $0 < \alpha < 1$ is a convergence factor.

Substituting into the error expression:

$$V_{\text{err}}(k+1) = V_{\text{ref}}(k) - V_{\text{actual}}(k+1) \tag{25}$$

$$= V_{\text{ref}}(k) - (V_{\text{actual}}(k) + \alpha \cdot V_{\text{err}}(k)) \tag{26}$$

$$= (1 - \alpha) \cdot V_{\text{err}}(k) \tag{27}$$

Substituting into the Lyapunov difference:

$$\Delta L(k) = \frac{1}{2} \left[(1-\alpha)^2 V_{\text{err}}(k)^T V_{\text{err}}(k) - V_{\text{err}}(k)^T V_{\text{err}}(k) \right] \tag{28}$$

$$= -\alpha(2-\alpha) \cdot \frac{1}{2} V_{\text{err}}(k)^T V_{\text{err}}(k) \tag{29}$$

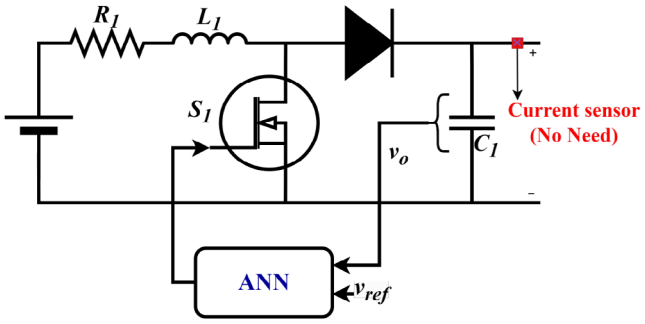

FIGURE 10 | Block diagram of proposed ANN controller implementation for single DER unit.

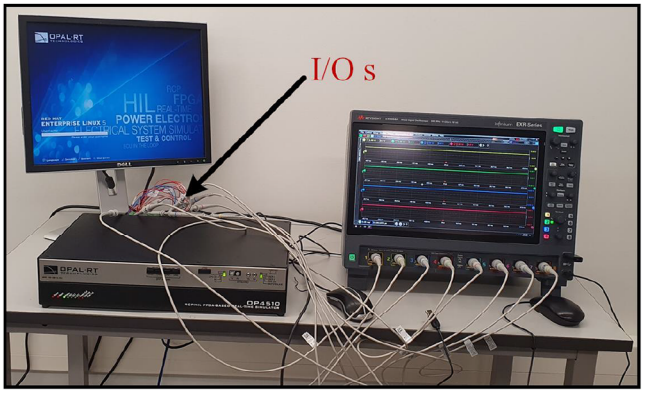

FIGURE 11 | Demonstration of HIL testing setup used to implement the DC MG.

Since $0 < \alpha < 1$, it follows that:

- $\Delta L(k) < 0$ for all $V_{\text{err}}(k) \neq 0$
- $\Delta L(k) = 0$ if and only if $V_{\text{err}}(k) = 0$

The quadratic Lyapunov function $L(k)$ represents the "energy" of the voltage error. The negative definite nature of $\Delta L(k)$ proves that this error energy decreases monotonically with each time step, eventually converging to zero. Furthermore, the controller's effectiveness is characterized by the convergence factor α, which determines the rate at which the system approaches the reference voltage.

5 | Results

Figure 10 illustrates the graphical implementation of the proposed reduced-sensor control technique for a single-step-up DC/DC converter. This technique requires only a voltage sensor to effectively regulate the output voltage at the PCC, eliminating the need for additional sensors and reducing overall system complexity and cost. Figure 11 depicts the hardware-in-the-loop (HIL) testing setup used to validate the proposed control technique. The setup includes an OPAL-RT 4510 real-time simulator, a graphical user interface (GUI) desktop, and a Keysight EXR058A 8-channel oscilloscope. The HIL platform operates in a hardware-synchronized mode, where analog inputs and outputs of the simulator are enabled and carefully configured for optimal

TABLE 4 | Simulation parameters.

Parameter	Value
DC input V_{in}	80 [V]
Inductor value L	4×10^{-5} [H]
Resistance value R	10×10^{-3} [Ω]
Capacitor C_f	600 [μF]
Line parameters Z_{12}	$R = 0.51$ [Ω], $L = 10$ [μH]
Line parameters Z_{13}	$R = 2$ [Ω], $L = 70$ [μH]
Line parameters Z_{24}	$R = 0.51$ [Ω], $L = 12.1$ [μH]
Line parameters Z_{43}	$R = 4$ [Ω], $L = 60$ [μH]
DC output V_{out}	100 [V]
PI parameters	$K_p = 0.00547$, $K_i = 7$

TABLE 5 | Controller performance comparison.

Controller	Settling time	Overshoot
PI	19.9 ms	180%
MPC	124 μs	0.445%
Proposed ANN	**99 μs**	**0.325%**

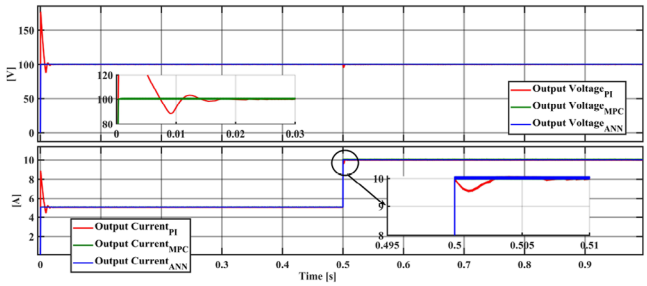

FIGURE 12 | Performance evaluation of PI and MPC and ANN-based voltage control.

performance. In this setup, each DER unit's output voltages and currents are measured using a simulator analog output measurement board. These signals are fed back into the simulator via an analog input board using wired connections. This approach ensures that critical real-world factors'such as system time delays, electrical noise, and signal interference–are accurately incorporated into the testing environment. Such fidelity allows for rigorous evaluation of the controller's performance under realistic operating conditions. The simulation parameters of the DC MG are given in Table 4. The performance comparison of different controllers in terms of overshoot and settling time is presented in Table 5. Figure 12 illustrates the performance of three different control techniques applied to step up DC-DC converter, comparing their output voltage and current responses. As shown in Figure 12, PI-based voltage control exhibits a relatively fast transient response but suffers from significant overshoot, which may lead to stability issues or stress on the system. The MPC-based voltage strategy improves with a more controlled rise and less overshoot, indicating better predictive adjustments and system stability. However, the proposed artificial neural network

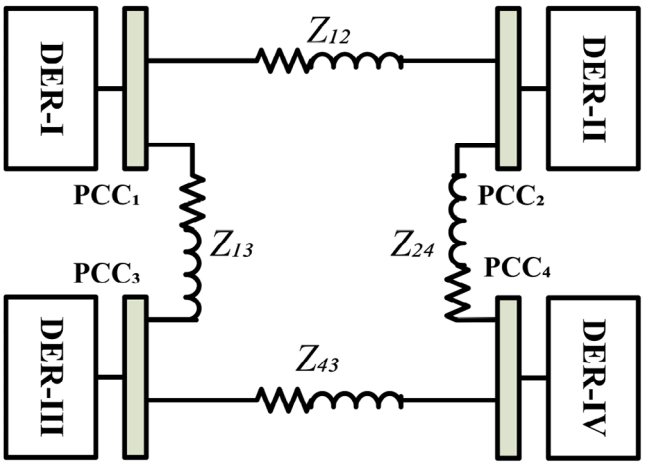

FIGURE 13 | The layout of the DC MG test bench system has four DER units connected in the ring structure.

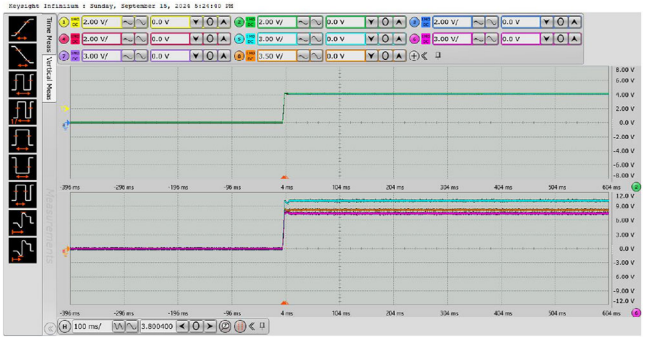

FIGURE 14 | The transient response evaluation of the proposed controller in DC MG test system.

control with reduced sensor outperforms both PI and MPC by achieving a rapid and precise rise to the desired levels with minimal overshoot and almost no fluctuation, displaying superior performance in maintaining consistent output. This quick settling time and the steady-state accuracy of the ANN suggest that it can better handle complex, dynamic conditions within the DC-DC converter's operation. The comparison between PI, MPC, and proposed ANN is carried out using MATLAB/SIMULINK.

5.1 | Voltage Tracking

In this case, we investigate and test the controller's performance and transient response while tracking the voltage reference. The controller performance is tested in an interconnected DC MG system, as presented in Figure 13. The test system consists of 4 DER units interconnected via transmission lines with their impedance. The DC test bench system is working in autonomous mode. Initially, the voltage of all DER units is set as per values expressed in Table 4.

As per the guidelines outlined in IEEE 1159-2019, the controller must ensure stability, achieve the intended transient and steady-state performance, and zero steady-state error in a closed-loop DC microgrid. The transient response of the proposed controller while tracking the voltage reference is shown in Figure 14.

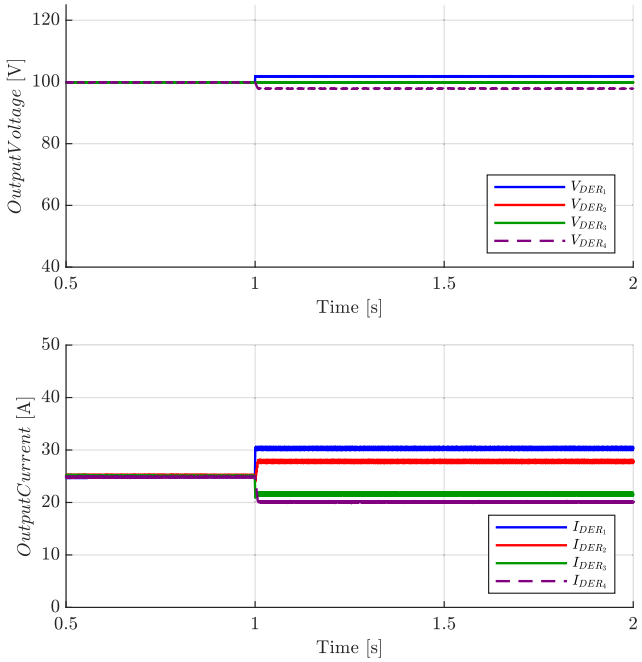

FIGURE 15 | Response of the DC microgrid to a reference voltage change for DER_1 and DER_4 at 1 s, with DER_1 adjusted from 100 V to 102 V and DER_4 from 100 V to 98 V. (a) Output voltage of all four DERs. (b) Output current of all DER Units connected in ring structure.

The observed waveform indicates that the studied controller effectively stabilizes the voltages of DER units according to their respective reference values without showing any undershooting or overshooting behavior.

Figure 15 illustrates the response of the proposed control regarding the change in voltage reference from 100 V to 102 V and 100 V to 98 V for DER_1 and DER_4 accordingly at $t = 1$ s. The response of the output voltage of DER_1 and DER_4 under the change of reference voltage is shown in Figure 15a. It can be observed from Figure 15 that the proposed controller remains stable against voltage reference change, attains the new reference without any transient and steady-state error, and follows the IEEE standards guideline. Furthermore, the output voltage of the neighbouring DGs of DER_1 and DER_4 remains stable and adjusts their current accordingly to meet the load connected to their respective PCC. It follows the reference without taking into account the disturbance and system impedance, as shown in Figure 15. So, the robustness and stability of the proposed controller are confirmed in these results against the change in reference voltage.

5.2 | PnP Functionality of DER Units

The plug-and-play capability of the DER units in MG is one of the essential requirements for the control system due to the intermittent nature of renewable energy. This test is validated rigorously in the real-time environment using the OPAL-RT Opal 4510 real-time simulator. The results are captured using a key sight EXR058A 8-channel oscilloscope. In this scenario, we investigate the performance of the proposed controller under the PnP functionality of the DERs. DER_4, connected to DER_2 and DER_3, is removed from the system at $t = 1$ s and is again

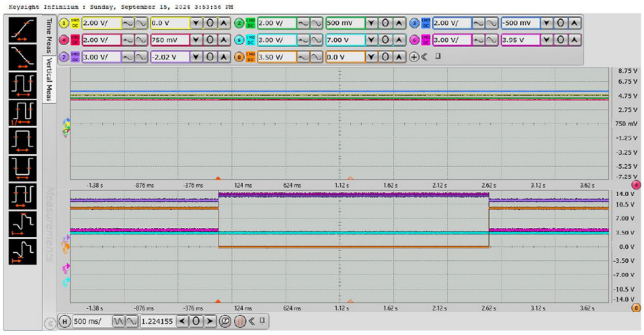

FIGURE 16 | Response of the DC microgrid following the removal of DER_4 from the system.

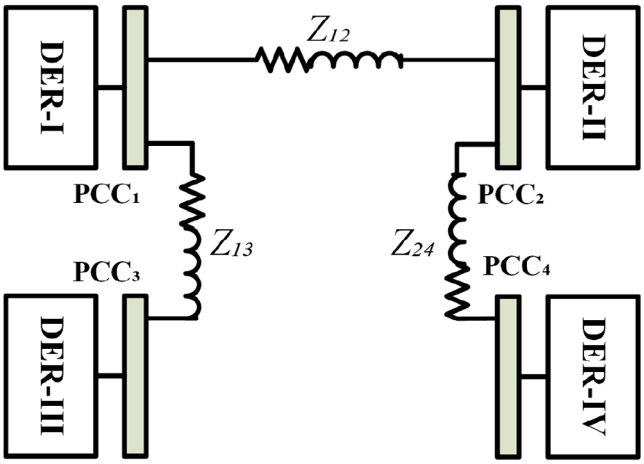

FIGURE 17 | DC microgrid layout after changing from the ring to radial distribution topology.

connected back into the microgrid at $t = 1.5$ s. However, the load at PCC4 remains connected all the time. This operation affected the adjacent DG units. The voltage and output current of all DERs are depicted in Figure 16. As shown in Figure 16, the DER_4 output current becomes zero. In contrast, the output current of the DER_2 and DER_3 increases to meet the load demand according to their capacity. At the same time, the voltage of all DGs remains stable without any disturbance and follows the reference with zero steady-state error. These results prove the robust performance of the proposed controller and the PnP capability in DC MG.

5.3 | Microgrid Topology Reconfiguration

This test case is performed to validate the stability and resilience of the proposed control system under different distribution network configurations. Initially, the configuration of the MG is in a ring-type distribution network. However, the line Z_{43} between DER_3 and DER_4 is disconnected, transforming the DC MG to a radial-type distribution network, as illustrated in Figure 17. Figure 18 presents the output voltages of all four DG at their PCCs. It is worth mentioning that the voltage of DERs remains stable and shows no fluctuation. The findings of this case depict the optimal performance of the designed controllers in response

FIGURE 18 | Output voltage of DER units against DC MG reconfiguration.

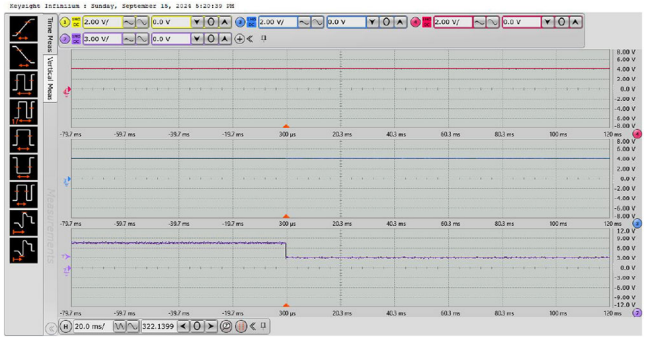

FIGURE 19 | Output voltage and current response of DER units under unknown load variation test.

to the variations resulting from uncertainties that affect the MG configurations.

5.4 | Adaptability to Unknown Load Variations

In this case, we investigate the performance of the developed controller against the load uncertainties. In addition, the system transient response and overshoot under varying load conditions are also studied. In the beginning, the loads mentioned in the table are connected at PCC3. At $t = 1$ s, the load is reduced to 1.25 kW at PCC3 as manifested in Figure 19. The 1st graph of the scope illustrates the output voltage of DER_1 and DER_4. The 2nd window of the oscilloscope shows the output voltage of DER_3, where the load is decreased, and the 3rd scope exhibits the output current of DER_3. It can be seen that with the decrease in load, the output current also decreases, but the voltage at all PCCs remains stable without any disturbance. Hence, the proposed controller shows robust behavior against unknown load variations.

5.5 | Controller Response to Parametric Variation

In this test, the sensitivity analysis of the proposed controller in a DC microgrid (MG) is conducted to demonstrate its stability against parametric variations. To evaluate the controller's robustness, the DC MG impedance is reduced by 20%, and the response of the DER units is analyzed. Figure 20 illustrates the output voltage and current of all four DER units, confirming that the controller maintains stability despite parametric variations.

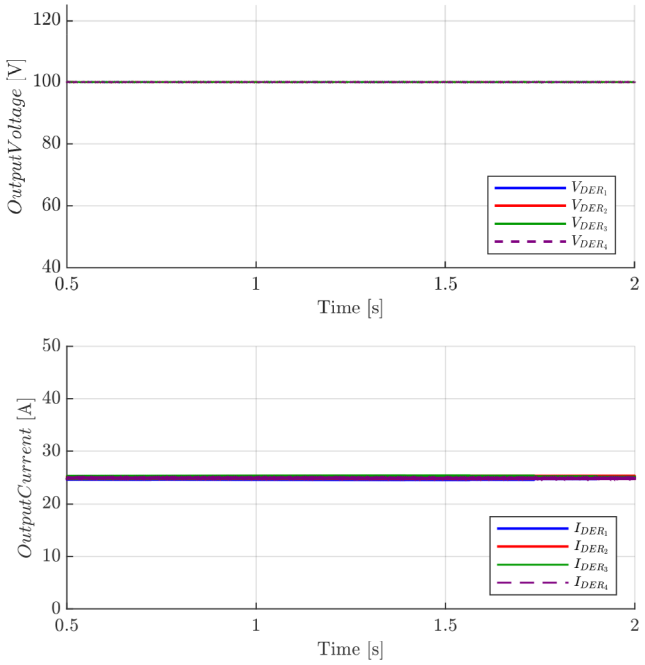

FIGURE 20 | Voltage and current response of DER units in a ring configuration under a 20% reduction in line impedance compared to values in Table 4.

6 | Conclusion

Due to the high variations in loads and nonlinear dynamics of the power system, regulating the DC-DC converter is a significant problem. This article presents a reduced sensor ANN-based voltage control approach for a DC-DC step-up converter as a DG. Initially, the model predictive voltage control is implemented as an expert to extract the data set for the ANN training. After the ANN has been trained on different parameters and loading conditions, The finely tuned reduced sensor ANN is implemented to control the DC-DC converter. The proposed control technique performs better in various aspects, such as DERs' plug-and-play (PnP) operation, parameter variation, topology reconfiguration, and load fluctuations. Lyapunov stability analysis is also carried out to demonstrate the stability of the system via numerical simulation. It is important to mention that the ANN is trained and tuned using data from a single converter. However, it has been applied to four-bus systems that incorporate line parameters to assess its effectiveness. The results indicate that the proposed controller performs well in all scenarios compared to the classical PI controller. The real-time hardware-in-loop results also validate the robust performance of the proposed control approach under different cases.

Author Contributions

Hussain Sarwar Khan: conceptualization, investigation, methodology, software, validation, writing – original draft. **Kimmo Kauhaniemi:** supervision, writing – review and editing.

Acknowledgements

This work is carried out in a project titled Smart Grid 2.0 with the financial support provided by Business Finland under Grant No.

1386/31/2022. The financial support provided by the funding organisation is highly acknowledged.

Open access publishing facilitated by Vaasan yliopisto, as part of the Wiley - FinELib agreement.

Conflicts of Interest

The authors declare no conflicts of interest.

Data Availability Statement

The data that support the findings of this study are available from the corresponding author upon reasonable request.

References

1. A. Anand, A. Ranjan, S. Devassy, B. K. Verma, S. K. Ram, and A. K. Dhakar, "Review of Hierarchical Control Strategies for dc Microgrid," *IET Renewable Power Generation* 14, no. 10 (2020): 1631–1640.

2. Mahdi Zolfaghari, Gevork B Gharehpetian, Miadreza Shafie-khah, and Joao PS Catalao, "Comprehensive Review on the Strategies for Controlling the Interconnection of ac and dc Microgrids," *International Journal of Electrical Power & Energy Systems* 136 (2022): 107742.

3. M. Mosayebi, M. Gheisarnejad, and M. H. Khooban, "An Intelligent Sliding Mode Control for Stabilization of Parallel Converters Feeding Cpls in dc-Microgrid," *IET Power Electronics* 15, no. 14 (2022): 1596–1606.

4. F. Ibanez, J. Echeverria, and L. Fontan, "Master–Slave dc Droop Control for Paralleling Auxiliary dc/dc Converters in Electric bus Applications," *IET Power Electronics* 10, no. 10 (2017): 1156–1164.

5. Y. Mi, J. Guo, S. Yu, et al., "A Power Sharing Strategy for Islanded dc Microgrid With Unmatched line Impedance and Local Load," *Electric Power Systems Research* 192 (2021): 106983.

6. N. Mohammed, L. Callegaro, M. Ciobotaru, and J. M. Guerrero, "Accurate Power Sharing for Islanded dc Microgrids Considering Mismatched Feeder Resistances," *Applied Energy* 340 (2023): 121060.

7. M. Saleh, Y. Esa, and A. A. Mohamed, "Communication-Based Control for dc Microgrids," *IEEE Transactions on Smart Grid* 10, no. 2 (2018): 2180–2195.

8. P. Montegiglio, G. Acciani, M. Dicorato, G. Forte, and F. Marasciuolo, "A Decentralized Power and bus Voltage Regulation Approach for dc Microgrids," *IEEE Transactions on Industry Applications* 59, no. 4 (2023): 4773–4785.

9. R. Jeyasenthil, T. Kobaku, B. Subudhi, S. Sahoo, and T. Dragicevic, "Design and Experimental Validation of Robust pid Control for a Power Converter in a dc Microgrid Application," in *Microgrid Cyberphysical Systems* (Elsevier, 2022), 89–114.

10. C.-F. Hsu, I.-F. Chung, C.-M. Lin, and C.-Y. Hsu, "Self-Regulating Fuzzy Control for Forward dc–dc Converters Using an 8-Bit Microcontroller," *IET Power Electronics* 2, no. 1 (2009): 1–13.

11. T.-F. Wu, C.-H. Chang, and Y.-H. Chen, "A Fuzzy-Logic-Controlled Single-Stage Converter for Pv-Powered Lighting System Applications," *IEEE Transactions on Industrial Electronics* 47, no. 2 (2000): 287–296.

12. T. Gupta, R. R. Boudreaux, R. M. Nelms, and J. Y. Hung, "Implementation of a Fuzzy Controller for dc-dc Converters Using an Inexpensive 8-b Microcontroller," *IEEE Transactions on Industrial Electronics* 44, no. 5 (1997): 661–669.

13. Zainab Ameer Al-Dabbagh and Salam Waley Shneen, "Neuro-Fuzzy Controller for a non-Linear Power Electronic dc-dc Boost Converters," *Journal of Robotics and Control (JRC)* 5, no. 5 (2024): 1479–1491.

14. S. Oucheriah and L. Guo, "Pwm-Based Adaptive Sliding-Mode Control for Boost dc–dc Converters," *IEEE Transactions on Industrial Electronics* 60, no. 8 (2012): 3291–3294.

15. H. S. Khan, K. S. Fuad, M. Karimi, and K. Kauhaniemi, "Fault Current Level Analysis of Future Microgrids With High Penetration Level of Power Electronic-Based Generation," in *2021 IEEE 9th International Conference on Smart Energy Grid Engineering (SEGE)* (IEEE, 2021), 48–53.

16. L. Cheng, P. Acuna, R. P. Aguilera, et al., "Model Predictive Control for dc–dc Boost Converters With Reduced-Prediction Horizon and Constant Switching Frequency," *IEEE Transactions on Power Electronics* 33, no. 10 (2017): 9064–9075.

17. S. R. Mohapatra and V. Agarwal, "An Advanced Voltage Support Scheme Considering the Impact of Zero-Sequence Voltage Under Microgrid Faults Using Model Predictive Control," *IEEE Transactions on Industrial Electronics* 67, no. 10 (2020): 8957–8968.

18. Y. Shan, J. Hu, K. W. Chan, Q. Fu, and J. M. Guerrero, "Model Predictive Control of Bidirectional dc–dc Converters and Ac/Dc Interlinking Converters–a New Control Method for Pv-Wind-Battery Microgrids," *IEEE Transactions on Sustainable Energy* 10, no. 4 (2018): 1823–1833.

19. Z. Karami, Q. Shafiee, Y. Khayat, M. Yaribeygi, T. Dragicevic, and H. Bevrani, "Decentralized Model Predictive Control of dc Microgrids With Constant Power Load," *IEEE Journal of Emerging and Selected Topics in Power Electronics* 9, no. 1 (IEEE, 2019): 451–460.

20. L. Chen, F. Gao, K. Shen, et al., "Predictive Control Based dc Microgrid Stabilization With the Dual Active Bridge Converter," *IEEE Transactions on Industrial Electronics* 67, no. 10 (2020): 8944–8956.

21. H. U. R. Habib, S. Wang, M. R. Elkadeem, and M. F. Elmorshedy, "Design Optimization and Model Predictive Control of a Standalone Hybrid Renewable Energy System: A Case Study on a Small Residential Load in Pakistan," *IEEE Access* 7 (2019): 117369–117390.

22. M. Cavus, A. Allahham, K. Adhikari, and D. Giaouris, "A Hybrid Method Based on Logic Predictive Controller for Flexible Hybrid Microgrid With Plug-And-Play Capabilities," *Applied Energy* 359 (2024): 122752.

23. N. Jin, S. Hu, C. Gan, and Z. Ling, "Finite States Model Predictive Control for Fault-Tolerant Operation of a Three-Phase Bidirectional AC/DC Converter Under Unbalanced Grid Voltages," *IEEE Transactions on Industrial Electronics* 65, no. 1 (2017): 819–829.

24. B.-R. Lin, "Power Converter Control Based on Neural and Fuzzy Methods," *Electric Power Systems Research* 35, no. 3 (1995): 193–206.

25. I. S. Mohamed, S. Rovetta, T. D. Do, T. Dragicević, and A. A. Z. Diab, "A Neural-Network-Based Model Predictive Control of Three-Phase Inverter With an Output lc Filter," *IEEE Access* 7 (2019): 124737–124749.

26. H. S. Khan, I. S. Mohamed, K. Kauhaniemi, and L. Liu, "Artificial Neural Network-Based Voltage Control of dc/dc Converter for dc Microgrid Applications," in *2021 6th IEEE Workshop on the Electronic Grid (eGRID)* (IEEE, 2021), 1–6.

27. S. Saadatmand, P. Shamsi, and M. Ferdowsi, "The Voltage Regulation of a Buck Converter Using a Neural Network Predictive Controller," in *2020 IEEE Texas Power and Energy Conference (TPEC)* (IEEE, 2020), 1–6.

28. S. Saadatmand, M. S. S. Nia, P. Shamsi, M. Ferdowsi, and D. C. Wunsch, "Neural Network Predictive Controller for Grid-Connected Virtual Synchronous Generator," in *2019 North American Power Symposium (NAPS)* (IEEE, 2019), 1–6.

29. A. N. Akpolat, M. R. Habibi, E. Dursun, A. E. Kuzucuoğlu, Y. Yang, T. Dragičević, and F. Blaabjerg, "Sensorless Control of dc Microgrid Based on Artificial Intelligence," *IEEE Transactions on Energy Conversion* 36, no. 3 (2020): 2319–2329.

30. M. Ahmed, A. Vahidnia, M. Datta, and L. Meegahapola, "An Adaptive Power Oscillation Damping Controller for a Hybrid AC/DC Microgrid," *IEEE Access* 8 (2020): 69482–69495.

31. S. Kanwal, M. Q. Rauf, B. Khan, and G. Mokryani, "Artificial Neural Network Assisted Robust Droop Control of Autonomous Microgrid," *IET Renewable Power Generation* 18, no. 7 (2024): 1346–1369.

32. A. Wang, M. Fei, D. Du, C. Peng, and K. Li, "Scalable Neural Network Control for Nonlinear dc Microgrids Under Plug-And-Play Operations," *IEEE Transactions on Industrial Informatics* 21, no. 5 (2025): 3849–3859.

33. H. S. Khan and K. Kauhaniemi, "Fpga Validated Advanced Learning-Based Voltage Control of dc/dc Converter Feeding Cpl in dc Microgrid

Applications," in *2023 IEEE 32nd International Symposium on Industrial Electronics (ISIE)* (IEEE, 2023), 1–6.

34. S. Zhao, F. Blaabjerg, and H. Wang, "An Overview of Artificial Intelligence Applications for Power Electronics," *IEEE Transactions on Power Electronics* 36, no. 4 (2021): 4633–4658.

35. A. N. Akpolat, E. Dursun, and A. E. Kuzucuoğlu, "Deep Learning-Aided Sensorless Control Approach for PV Converters in dc Nanogrids," *IEEE Access* 9 (2021): 106641–106654.

36. A. H. EL-Ebiary, M. I. Marei, M. A. Attia, and M. Mokhtar, "A Sensorless Cyberattacks Mitigation Technique Based on Braided Lyapunov State Observer," *Electric Power Systems Research* 235 (2024): 110881.

37. N. Obeidi, M. Kermadi, B. Belmadani, A. Allag, L. Achour, and S. Mekhilef, "A Current Sensorless Control of Buck-Boost Converter for Maximum Power Point Tracking in Photovoltaic Applications," *Energies* 15, no. 20 (2022): 7811.

38. M. Tavan, K. Sabahi, M. Shahparasti, A. Hajizadeh, M. Soltani, and M. Savaghebi, "Sensorless Control of a Single-Phase Ac–Dc Boost Converter Without Measuring Input Voltage and Current," *IEEE Access* 11 (2023): 59059–59070.

39. S. K. Kim and C. K. Ahn, "Proportional-Derivative Voltage Control With Active Damping for dc/dc Boost Converters Via Current Sensorless Approach," *IEEE Transactions on Circuits and Systems II: Express Briefs* 68, no. 2 (2020): 737–741.

40. M. Tucci, S. Riverso, J. C. Vasquez, J. M. Guerrero, and G. Ferrari-Trecate, "A Decentralized Scalable Approach To Voltage Control of dc Islanded Microgrids," *IEEE Transactions on Control Systems Technology* 24, no. 6 (2016): 1965–1979.

41. D. Wang, Z. J. Shen, X. Yin, et al., "Model Predictive Control Using Artificial Neural Network for Power Converters," *IEEE Transactions on Industrial Electronics* 69, no. 4 (2021): 3689–3699.

42. M. S. Sadabadi, Q. Shafiee, and A. Karimi, "Plug-And-Play Robust Voltage Control of dc Microgrids," *IEEE Transactions on Smart Grid* 9, no. 6 (2017): 6886–6896.

43. L. Chen and X. Wang, "Enhanced Mppt Method Based on Ann-Assisted Sequential Monte–Carlo and Quickest Change Detection," *IET Smart Grid* 2, no. 4 (2019): 635–644.

44. M. R. Habibi, H. R. Baghaee, F. Blaabjerg, and T. Dragićević, "Secure mpc/ann-Based False Data Injection Cyber-Attack Detection and Mitigation in dc Microgrids," *IEEE Systems Journal* 16, no. 1 (2021): 1487–1498.

45. K. Hornik, "Approximation Capabilities of Multilayer Feedforward Networks," *Neural Networks* 4, no. 2 (1991): 251–257.

46. Julian Berberich, Johannes Köhler, Matthias A Müller, and Frank Allgöwer, "Data-Driven Model Predictive Control With Stability and Robustness Guarantees," *IEEE Transactions on Automatic Control* 66, no. 4 (2021): 1702–1717.

47. Joscha Bongard, Julian Berberich, Johannes Köhler, and Frank Allgöwer, "Robust Stability Analysis of a Simple Data-Driven Model Predictive Control Approach," *IEEE Transactions on Automatic Control* 68, no. 5 (2023): 2625–2637.